AD621028

# AIR FORCE INSTITUTE OF TECHNOLOGY

AIR UNIVERSITY
UNITED STATES AIR FORCE

INVESTIGATION OF THE EFFECT OF
PLUG TRANSLATION ON THE THRUST
VECTOR OF A MACH [illegible] PLUG NOZZLE

GAM [illegible]

RICHARD F. ELLINGSON
CAPT USAF

CLEARINGHOUSE
FOR FEDERAL SCIENTIFIC AND
TECHNICAL INFORMATION
Hardcopy Microfiche
$2.00 $0.50 47 pp
ARCHIVE COPY

## SCHOOL OF ENGINEERING

WRIGHT-PATTERSON AIR FORCE BASE, OHIO

DDC
SEP 27 1965
TISIA D

# INVESTIGATION OF THE EFFECT OF PLUG TRANSLATION ON THE THRUST VECTOR OF A MACH 3 PLUG NOZZLE

THESIS

Presented to the Faculty of the School of Engineering of

the Air Force Institute of Technology

Air University

in Partial Fulfillment of the

Requirements for the Degree of

Master of Science

by

Richard K. Ellingson, B.S.

Capt USAF

Graduate Aerospace-Mechanical Engineering

June 1965

## Acknowledgements

I wish to express my appreciation to my thesis advisor, Major Leonard A. Hamilton, for his aid, advice and encouragement; and to Mr. Richard Brown for his able and willing assistance in the laboratory. Most especially I must acknowledge my debt of gratitude to my wife, Elizabeth, and my children for their patience and understanding, and for the sacrifices they have made in order that I may more effectively pursue my studies and work.

Richard K. Ellingson

## Contents


| | Page |
|---|---|
| Acknowledgements | ii |
| List of Figures | v |
| List of Symbols and Subscripts | vi |
| Summary | vii |
| I. Introduction | 1 |
| Background | 1 |
| Thrust Vectoring | 2 |
| Theoretical Model | 3 |
| Analytical Considerations | 3 |
| Objective | 5 |
| Experimental Investigation | 5 |
| II. Experimental Investigation | 6 |
| Apparatus | 6 |
| Air Supply | 6 |
| Blow-Down Wind Tunnel | 6 |
| Instrumentation | 7 |
| Schlieren Optical Equipment | 8 |
| Model | 8 |
| Test Program | 9 |
| Run Procedures | 9 |
| Run Reproducibility | 10 |
| Schlieren Photographs | 10 |
| Experimental Observations | 11 |
| Flow-Meter | 11 |
| Stagnation Pressure | 11 |
| Throat Pressure | 11 |
| Data Reduction | 12 |
| Determination of Pressure Ratios to be Evaluated | 12 |
| Mass Flow Rate | 12 |
| Axial Force Calculations | 12 |
| Transverse Force Calculations | 13 |
| Determination of Angle $\alpha$ | 13 |
| Determination of $C_{f_p}$ | 14 |
| Experimental Findings | 14 |
| Wall Pressure Distribution for the Ideal Plug | 14 |
| Wall Pressure Distribution for the Translated Plug | 15 |
| III. Discussion of Results and Comparisons | 16 |
| The Axial Thrust Coefficient, $C_{f_p}$ | 16 |
| Analysis of Thrust Vectoring Mechanism | 17 |

Page

IV. Conclusions and Recommendations . . . . . 19

Bibliography . . . . . 20

Table I: Pertinent Information on Transducers, Visicorder and Amplifiers . . . . . 39

Vita . . . . . 40

## List of Figures


| Figure | | Page |
|---|---|---|
| 1 | Sketch of Three-Dimensional Plug Nozzle with Translating Plug | 21 |
| 2 | Two-Dimensional Plug Nozzle with Translating Plug | 22 |
| 3 | General Arrangement of Apparatus | 23 |
| 4 | Schematic of Air Supply and Blow-Down Wind Tunnel | 24 |
| 5 | Test Section and Plug Nozzles | 25 |
| 6 | Dimensions of Plug Nozzles | 26 |
| 7 | Plug Nozzle Assembly | 27 |
| 8 | Schlieren Photographs of Ideal Plug Nozzle | 28 |
| 9 | Schlieren Photographs of Translated Plug Nozzle | 29 |
| 10 | Experimental Plug Wall Pressure Distribution for Ideal and Translated Plug, $P_o/P_b = 60$ | 30 |
| 11 | Experimental Plug Wall Pressure Distribution for Ideal and Translated Plug, $P_o/P_b = 37$ | 31 |
| 12 | Experimental Plug Wall Pressure Distribution for Ideal and Translated Plug, $P_o/P_b = 30$ | 32 |
| 13 | Experimental Plug Wall Pressure Distribution for Ideal and Translated Plug, $P_o/P_b = 18$ | 33 |
| 14 | Experimental Plug Wall Pressure Distribution for Ideal and Translated Plug, $P_o/P_b = 14$ | 34 |
| 15 | Experimental Plug Wall Pressure Distribution for Ideal and Translated Plug, $P_o/P_b = 10$ | 35 |
| 16 | Variation of Thrust Vectoring with Pressure Ratio | 36 |
| 17 | Variation of Axial Thrust Coefficient, $C_{f_p}$, with Pressure Ratio | 37 |
| 18 | Comparison Between Experimental Data and Method of Characteristics, $P_o/P_b = 37$ | 38 |

## List of Symbols and Subscripts

### Symbols

| | |
|---|---|
| $A$ | Area, $In^2$ |
| $Cf_p$ | Plug axial thrust coefficient (see page 4) |
| $dA_w$ | Element of plug wall area |
| $F$ | Thrust, $lb_f$ |
| $g_c$ | Dimensional conversion factor, $32.174 \frac{ft\ lb_m}{lb_f\ sec^2}$ |
| $k$ | Ratio of specific heats |
| $\dot{m}$ | Mass flow rate, $lb_m/sec$ |
| $P$ | Pressure, psia |
| $R$ | Gas constant for air, $53.3 \frac{ft\ lb_f}{lb_m\ {}^oR}$ |
| $T$ | Temperature, $^oR$ |
| $V$ | Velocity, ft/sec |
| $X/L$ | Ratio of axial distance along the plug to plug length |
| $\alpha$ | Angle between thrust vector and axial direction |
| $\beta$ | Angle of nozzle lip to axial direction |
| $\theta$ | Local angle between plug wall and axial direction |

### Subscripts

| | |
|---|---|
| a | Ambient conditions |
| b | Back pressure existing in test chamber (ambient) |
| t | Throat conditions |
| T | Transverse direction (see Fig. 2) |
| w | Condition on plug wall |
| x | Axial direction (see Fig. 2) |
| o | Stagnation conditions |
| 1 | Properties of side 1 (see Fig. 2) |
| 2 | Properties of side 2 (see Fig. 2) |

## Summary

An experimental investigation was made of a convergent plug exhaust nozzle to determine if effective thrust vectoring could be achieved through the use of a translating plug which travels in plane motion across a base region of slightly increased diameter.

A previous two-dimensional study showed that a pressure differential existed across the plug as the plug was moved from the centered position. The thrust vectoring created by this pressure differential was insignificant. However, there were indications that effective thrust vectoring could be obtained for higher pressure ratios than the maximum of 6.2 obtained in that investigation.

The objective of this study was to determine if effective thrust vectoring could be obtained at higher pressure ratios.

To achieve the objective, a two-dimensional, Mach 3, plug nozzle, with a design pressure ratio of 36.7, was tested in cold flow in a blow-down wind tunnel. Three configurations, corresponding to ideal, centered, and fully translated nozzles, were tested over a range of nozzle pressure ratios from 10 to 60. Pressure transducers and a Visicorder were utilized to measure the necessary pressures for evaluation of the transverse and axial components of thrust. Flow visualization was accomplished by the use of a Schlieren optical system.

Results showed that when operating at pressure ratios below the design value the amount and direction of thrust vectoring obtained was a strong function of the pressure ratio. For underexpanded operation the thrust vectoring was found to be nearly independent of the pressure ratio, but of too small a magnitude to be significant. The axial thrust was materially reduced by the step in both plugs.

# INVESTIGATION OF THE EFFECT OF PLUG TRANSLATION ON THE THRUST VECTOR OF A MACH 3 PLUG NOZZLE

## I. Introduction

### Background

A plug nozzle is characterized by having a central conical plug that controls the supersonic expansion of the exhaust jet. There are several variations of the basic plug nozzle, but the only type considered here is one where the expansion occurs without external walls. This type is generally referred to as a convergent plug nozzle. The nozzle is designed to produce ideal isentropic expansion of the exhaust jet with an axial velocity vector at a particular ratio of chamber to ambient pressure.

The outer jet boundary is not confined within fixed walls, but is allowed to expand until the pressure in the exhaust jet reaches ambient pressure. At low altitudes, where the nozzle is operating below the design pressure ratio, the free jet boundary is redirected by the ambient pressure and produces a nearly axial velocity vector. Thus, compensation for overexpansion is obtained, and the nozzle performance tends to stay nearly constant up to the design pressure ratio.

In contrast with the plug nozzle, the conventional convergent-divergent nozzle with its fixed outer walls, does not compensate for overexpansion. At pressure ratios below the design value the convergent-divergent nozzle expands the exhaust jet to a pressure which is below ambient pressure. Thus a part of the internal wall of the nozzle

is being acted upon by a pressure that is below ambient, and a loss of thrust is encountered. Thus, at low altitudes (below design pressure ratio) the performance of the plug nozzle exceeds that of the conventional nozzle (Ref 1). At higher altitudes, where the pressure ratio is equal to or greater than design, the performance of the plug nozzle equals that of a conventional nozzle. One problem, which has limited the utilization of the plug nozzle for rocket application, is thrust vectoring.

## Thrust Vectoring

Thrust vectoring of rocket engines with conventional nozzles is often accomplished by gimballing the entire engine. This method is not practical for engines equipped with plug nozzles however, since the plug nozzle reaches its maximum diameter at the throat which is near the aft end of the vehicle, and such a method would require complicated attachment and gimballing mechanisms.

Berman (Ref 2) suggests a method where only the central plug is gimballed. This procedure creates asymmetrical flow of the exhaust jet about the plug and thrust vectoring is obtained. This method would also require heavy and complicated support and activating mechanisms, and there would probably be a performance reduction since the throat area would be varied. Barnes (Ref 3) suggested a method that may reduce the stresses on the activating mechanism and simplify the support system. This method consists of moving only the portion of the plug that extends downstream of the throat. The external portion of the plug is not gimballed but moves in two-dimensional translation across a base plug of slightly greater dimensions (see Fig. 1). With the plug in the

centered position an equal step or setback exists around the circumference of the plug. As the plug is translated from the center, the side with decreasing setback will approach the ideal configuration. The losses due to flow separation will decrease and the thrust will increase. For the side with the increasing setback, the plug departs further from the ideal configuration, resulting in a reduction in thrust. The net effect of plug translation is the creation of a pressure differential across the plug.

## Theoretical Model

If any cross flow created by a pressure differential existing across the plug nozzle is disregarded, the flow about a conical plug nozzle may be considered to be nearly two-dimensional for an incremental area on the plug circumference. A two-dimensional study will therefore retain the basic idea of thrust vectoring through plug translation and will allow for a simpler experimental study.

## Analytical Considerations

Applying the momentum equation in vector form with the assumption of a straight sonic line and constant properties at the throat, the thrust equation becomes

$$\vec{F} = \frac{\dot{m}}{g_c}\vec{V}_t + (P_t - P_a)\vec{A}_t + \int (P_w - P_a)d\vec{A}_w \qquad (1)$$

The first two terms are positive and represent the jet thrust which acts on the nozzle at the throat. The third term is a summation of the pressure forces acting on the surface of the plug, created by the expansion of the exhaust jet.

If the throat area and angle $\beta$ are the same for both sides of the

plug nozzle, but allowance is made for varying properties (see Fig. 2), the two-dimensional thrust equation may be divided into two components, axial and transverse. The axial thrust is given by

$$F_x = \frac{(\dot{m}_1 V_{t1} + \dot{m}_2 V_{t2})}{g_c} \cos\beta + (P_{t1} + P_{t2} - 2P_a)A_t \cos\beta +$$

$$\int (P_{w1} - P_a) \sin\theta_1 \, dA_{w1} + \int (P_{w2} - P_a) \sin\theta_2 \, dA_{w2} \qquad (2)$$

The transverse force equation then becomes

$$F_T = \frac{(-\dot{m}_1 V_{t1} + \dot{m}_2 V_{t2})}{g_c} \sin\beta + (-P_{t1} + P_{t2})A_t \sin\beta -$$

$$\int (P_{w1} - P_a) dA_{w1} \cos\theta_1 + \int (P_{w2} - P_a) dA_{w2} \cos\theta_2 \qquad (3)$$

The first two terms in equations 2 and 3 may be determined from measured conditions at the throat and known physical dimensions of the nozzle. To evaluate the integral terms in equations 2 and 3 it is necessary to know the pressure at every point along the plug wall contour.

The amount of thrust vectoring produced by the translated plug may be evaluated by forming the ratio of transverse to axial forces. This ratio aids in defining the angle $\alpha$ which is the angle the total thrust vector makes with the axial direction. The angle $\alpha$ appears to be a function of the amount of plug translation, and the nozzle pressure ratio. The step in the plug may cause an undesired reduction in the axial thrust. A dimensionless thrust coefficient $C_{f_p}$ is defined to express the efficiency of the translated plug in producing axial thrust. A plug which has no step and, thus conforms to the ideal

configuration will be taken as reference. $C_{f_p}$ is then defined as the axial thrust for the translated plug divided by the axial thrust for the plug which contains no step. Barnes (Ref 3) performed a theoretical and experimental study of thrust vectoring with a translatable plug nozzle. This study was conducted at relatively low pressure ratios (maximum of 6.60) and with a nozzle designed for an exit Mach number of 2. Barnes found that at low pressure ratios the amount of thrust vectoring obtained was not significant, but that there seemed to be evidence of increased thrust vectoring with increasing pressure ratios. He also found that a normal shock occurred in the flow over the translated plug. This normal shock appeared to strongly influence the amount of thrust vectoring.

## Objective

The objective of this study was to investigate the possibility of obtaining significant thrust vectoring with a translatable plug nozzle at higher pressure ratios.

Experimental Investigation. Three models corresponding to three possible plug positions (ideal, centered and fully translated) were built and tested in a blow-down wind tunnel. Pressure transducers were used to obtain the necessary static pressures. Equations 2 and 3 were used to evaluate the performance of the nozzles. Schlieren optical techniques were employed to obtain flow visualization.

## II. Experimental Investigation

### Apparatus

The general arrangement of test equipment in the laboratory is shown in Fig. 3. Facilities of the Mechanical Engineering Laboratory of the Air Force Institute of Technology were used for this experiment.

Air Supply. One compressor rated at 100 psi gage provided oil-free air for this experiment. With the nozzle exhausting to atmospheric pressure (approximately 14.3 psia) the maximum pressure ratio would be about 8, which is insufficient to meet the objective of this study. Therefore, the air supply was used with a blow-down wind tunnel in order to achieve the desired pressure ratios (see Figs. 3 and 4).

Blow-Down Wind Tunnel. The blow-down wind tunnel allowed pressure ratios of 10 to 70 to be obtained. The blow-down wind tunnel (see Fig. 5a) has a 1 inch wide test section. Glass sidewalls, suitable for Schlieren, provide a visible portion of 4 inches high and 14 inches long for flow visualization. For a complete description of the blow-down tunnel see Reference 4.

The blow-down tunnel exhausts into two tanks with a total volume of 450 $ft^3$. These tanks may be evacuated to a low pressure, thus obtaining the desired pressure ratios. These tanks are designed for only a slight over pressure (pressure inside greater than atmospheric). A vacuum pump was available to evacuate the low pressure tanks to 0.4 psia in approximately 40 minutes. This low pressure permits an initial starting pressure ratio $P_o/P_b$ of approximately 160. Note that $P_b$ is defined as the back pressure existing in the test section and evacuated tanks, and corresponds to ambient pressure for an actual

rocket. In actual runs it was found that the pressure ratio dropped to approximately 70 before supersonic flow was obtained and stabilized. For the rest of the run time the pressure ratio decreased linearly with time. The run time was approximately 21 seconds; at this time the run had to be terminated to avoid an over pressure on the low pressure tanks.

Instrumentation. Twelve pressure transducers were used to record pressure readings. Two 0-100 psid transducers were used to record upstream and differential pressures necessary for mass flow computation. Three 0-100 psia transducers were used to measure throat and stagnation pressures. The back pressure was measured with an 0-30 psia transducer. The nozzle wall pressures were measured with six transducers (three 0-35 psia and three 0-50 psia). All transducers were of the potentiometer type. Transducer voltage outputs were recorded by using two 6 channel galvanometer amplifiers and a 12 channel Visicorder. The Visicorder provided an immediate print of transducer output on sensitized paper. See Table I for further information on transducers, amplifiers and Visicorder. A 24 volt battery with a variable slide wire resistor was used to supply a constant 12 volt reference to the transducers. A voltmeter was used to measure the reference voltage.

The entire system, consisting of transducers, amplifiers, Visicorder and necessary wiring, was calibrated before actual runs were accomplished. An 0-200 inch mercury dial gage graduated in 0.2 inch increments was used to calibrate the system for pressures greater than atmospheric. A mercury U-tube manometer was used for calibration below atmospheric pressure. A maximum allowable deflection of 1 inch on the Visicorder allowed for calibrations ranging from 190 inches of mercury per inch of galvanometer deflection (for orifice upstream

pressure) to 40 inches of mercury per inch of galvanometer deflection (for back pressure). A check on calibration was possible before each run. This was done by obtaining and comparing Visicorder readings at atmospheric pressure and after evacuation of the test chamber. All transducers and galvanometers proved to be linear within ± 1 1/2% over their respective ranges.

The flow-meter consisted of a 1.00 inch diameter flat plate orifice placed in the 2 inch diameter air supply line. The flow-meter installation conformed to the standards of the ASME (Ref 5). Temperature upstream of the flow-meter was measured with a copper-constantan thermocouple placed just upstream of the orifice. Nozzle stagnation temperature was considered to be closely approximated by this temperature.

Schlieren Optical Equipment. A Schlieren optical system was used to observe the nozzle flow. Photographs were taken with a bellows type camera having a Polaroid film holder. A spark lamp was used for the light source. Polaroid type 42 film was used throughout. All photographs presented in this report were taken with the knife edge horizontal.

Model. To allow for the exit of tubing from the test section of the blow-down tunnel it was necessary to design three configurations of the translatable plug nozzle (see Figs. 6 and 7). The three configurations designed and tested were:

1) Translated (full setback)
2) Centered (1/2 setback)
3) Ideal (no setback)

The ideal configuration was used as a reference. The centered configuration was used to determine the effect of the setback on axial

thrust when no thrust vectoring is desired. The fully translated plug was used to determine the amount of thrust vectoring obtainable and the effect of the setback on axial thrust. The overall dimensions of the nozzle were restricted by the test section dimensions and air supply. Throat dimensions of 1 inch by 0.4 inch were chosen. The three nozzles were made of wood and were identical upstream of the throat. The design of the base differs from that of a normal plug nozzle and was necessary to allow fitting to the blow-down wind tunnel test section. A constantly converging area was maintained up to the throat. The plug contours downstream of the throat were identically designed (except for the setback) by the method of characteristics (Ref 6) to give Prandtl-Meyer expansion about a lip at a pressure ratio of 36.7. At this pressure ratio the exit jet flows past the plug apex at a Mach number of 3. A setback of 7/16 inch for the translated plug was chosen to allow comparison with Barnes' results. The step for the centered plug then became 7/32 inch. A cavity was carved into one side of the plugs to accommodate the tubing for measuring the plug wall pressure. The cavity was filled with nonshrinking plastic after the tubing was installed. The nozzle lip was made of aluminum and a pressure tap was installed to measure throat pressure.

## Test Program

The three nozzle configurations were tested over a range of pressure ratios of from approximately 8 to 70. Data was evaluated at pressure ratios of 10, 14, 18, 30, 36.7 and 60.

Run Procedures. A typical run involved the following operations. The low pressure tanks were evacuated and the value of the pressure was

recorded on the Visicorder. The pressure upstream of the orifice was recorded prior to starting the compressor. This provided a reference to obtain the amount of galvanometer deflection during the run. The compressor was then started and allowed to build to near maximum pressure (just prior to compressor shut off). The Visicorder was turned on and the run was started by use of a quick acting valve on the high pressure line. The camera shutter was activated after a preselected time of operation and the temperature upstream of the flow-meter, which was assumed to be nozzle stagnation temperature, was determined by a potentiometer reading. A mercury U-tube manometer was observed to determine when the test chamber pressure was approaching atmospheric, at which time the valve was closed, terminating the run. The assumption that the total temperature of the orifice was the same as that in the settling chamber was checked and was found to be correct within 10°F

Run Reproducibility. As there were 10 wall static pressure taps and only 5 transducers available (one transducer was used to measure pressure in the setback) it was necessary to interchange the pressure transducers. Three runs were made for each location of the static wall pressure transducers and the pressures were averaged. The individual runs were reproducible to within ± 5% of the average.

Schlieren Photographs. Schlieren photographs were taken of the three nozzle configurations, and typical photographs are shown in Figs. 8 and 9. Photographs of the centered plug were found to be nearly identical to those of the translated plug and were not included. Note that although the knife edge was horizontal for all runs, those for the ideal configuration had the knife edge pointing down while for the translated plug the knife edge was pointing up.

Experimental Observations

Flow-Meter. The pressure upstream of the orifice varied by less than 1 psi (±1.2%) from an average value for the three nozzle configurations (for a particular pressure ratio). The pressure drop across the orifice varied by less than 0.35 psi (±2%) from the average. These variations were small enough to allow the averages to be used for mass flow rate computations.

Stagnation Pressure. The nozzle stagnation pressure was within 1.5 psi (±2%) of the average for the three nozzle configurations. An average was used in the computations.

Throat Pressure. Two pressure taps, one on the lip and one on the plug body, were used to measure throat pressure. The observed throat pressure measured at the nozzle lip was found to be within 1 psi (±2%) for the three nozzle configurations. The throat pressure measured on the plug body for the translated and centered plugs was consistently 13% below the theoretical throat pressure for all pressure ratios. This phenomenon was probably caused by premature supersonic expansion around the plug upstream of the throat, a condition which was noted in Reference 7. Thus a curved sonic line probably exists at the throat and equation 1 would be invalid (straight sonic line assumed at the throat). In view of the difficulty in obtaining the actual throat pressure distribution an average of the lip and plug throat pressures was used in the computations. The throat pressure, measured on the plug body, for the ideal configuration was approximately 4% above the theoretical throat pressure for all pressure ratios. The average of the lip and throat pressures was again used for the computation. The throat pressure, measured on the plug body for the ideal configuration,

was approximately 8 psi (17%) above the throat pressure of the centered and translated plug. No conclusive reason for premature expansion not occurring for the ideal plug could be reached.

## Data Reduction

Determination of Pressure Ratios to be Evaluated. So as to obtain useful data it was necessary to evaluate the three nozzle configurations at the same pressure ratio. Ideally the three nozzle configurations would be evaluated for steady flow, but as steady flow is never actually obtained in a blow-down tunnel without an upstream pressure regulator, it was necessary to pick a time interval for the evaluation of the data in which the pressure readings remained nearly constant. This limited the number of pressure ratios that were available for evaluation.

Mass Flow Rate. The nozzle mass flow rate was calculated from recorded flow-meter data using the standard ASME equations found in Reference 5. The mass flow rate varied linearly with pressure ratios from 0.82 to 0.85 lbm/sec.

Axial Force Calculations. By use of the continuity equation and isentropic relationships the throat velocity may be expressed in the form:

$$V_t = \frac{\dot{m}R}{A_t} \frac{T_o}{P_o} \left(\frac{P_o}{P_t}\right)^{1/k} \tag{4}$$

Insertion of equation 4 into the axial thrust equation 2 gives

$$F_x = \frac{[\dot{m}_1{}^2 T_{o1}(P_{t1})^{-1/k} + \dot{m}_2{}^2 T_{o2}(P_{t2})^{-1/k}]}{g_c} \frac{P_o^{\frac{1-k}{k}} R\cos\beta}{A_t} + (P_{t1}+P_{t2}-2P_a)A_t \cos\beta +$$

$$\int (P_{w1}-P_a) \sin\theta_1 \, dA_{w1} + \int (P_{w2}-P_a) \sin\theta_2 \, dA_{w2} \qquad (5)$$

The measured values of $\dot{m}$, $P_o$, and $P_t$ were used together with the known values of $A_t$ and $\beta$ to evaluate the non-integral terms of equation 5. The axial plug wall force for each of the configurations was obtained by graphical integration. A graph of plug wall pressure as a function of plug height will account for the local wall angle $\theta$. The curves were mechanically integrated with a polar planimeter. The axial force produced by the step was included in the integrations, but the force produced by the plug end was not included as there were an insufficient number of transducers to measure this pressure.

Transverse Force Calculations. By insertion of equation 4 into equation 3 the transverse force is given by:

$$F_T = \frac{[-\dot{m}_1{}^2 T_{o1}(P_{t1})^{-1/k} + \dot{m}_2{}^2 T_{o2}(P_{t2})^{-1/k}]}{g_c} \frac{P_o^{\frac{1-k}{k}} R\sin\beta}{A_t} + (P_{t1}-P_{t2})A_t \sin\beta -$$

$$\int (P_{w1}-P_a)dA_{w1} \cos\theta_1 + \int (P_{w2}-P_a)dA_{w2} \cos\theta_2 \qquad (6)$$

The non-integral terms were evaluated in the same manner as those for axial thrust. The plug wall force was obtained by mechanical integration of curves giving plug wall pressure as a function of plug axial length (see Figs. 10 through 15).

Determination of Angle $\alpha$. Angle $\alpha$ is defined as the angle the

total thrust vector $\vec{F}$ makes with the axial direction. For these computations subscript (1) in equations 5 and 6 was for the ideal nozzle while subscript (2) was for the translated plug. Therefore, $\alpha$ may be found from:

$$\alpha = \tan^{-1} \frac{F_T}{F_x} \tag{7}$$

A curve showing $\alpha$ as a function of pressure ratio is given in Fig. 16. Note that the direction of the transverse force has been assumed as in Fig. 2. Consequently, a negative sign indicates a transverse force in the opposite direction.

Determination of $C_{f_p}$. The dimensionless thrust coefficient $C_{f_p}$ is defined as the axial thrust of the stepped plug nozzle divided by the axial thrust of the ideal plug nozzle.

Equation 5 was used in its given form for the calculation of the axial thrust of the translated plug. The thrust of the ideal plug nozzle was obtained by doubling equation 5 with subscript (2) deleted (see Fig. 2). The axial thrust for the centered plug was obtained in the same manner except with subscript (1) deleted. A curve showing $C_{f_p}$ as a function of pressure ratio is shown in Fig. 17.

## Experimental Findings

Wall Pressure Distribution for the Ideal Plug. The variation of the wall pressure with pressure ratio is shown in Figs. 10 through 15. At the design pressure ratio, and for pressure ratios greater than design, the plug expands the flow until the design pressure is reached at the plug apex. For pressure ratios below design the flow is expanded until a pressure near ambient is reached on the plug wall upstream of the

apex, and compressive turning is then required for the flow to follow the plug contour (Ref 7:5). A curve of the theoretical wall pressure distribution, obtained from method of characteristics (Ref 6) is shown in Fig. 18 along with the experimental data points.

Wall Pressure Distribution for the Translated Plug. For pressure ratios greater than design (see Figs. 10 and 11) the pressure distribution curve shows three regions. The first is a low pressure region existing in the setback and is caused by flow separation at the throat. An oblique shock wave is then created as the flow reattaches to the wall as can be seen by the steep pressure rise. The flow then expands along the plug contour. As the pressure ratio drops to design or slightly below, a pressure rise occurs near the end of the plug as shown in Fig. 12. This pressure rise is created by an oblique shock. Schlieren photographs (see Fig. 9) show this oblique shock to be caused by expansion waves being reflected off the jet boundary (as compression waves) which coalesce into an oblique shock near the plug wall. This oblique shock then moves upstream with decreasing pressure ratio as may be seen from the Schlieren photographs and Figs. 12 through 15. Behind the oblique shock the flow again expands as may be seen from the wall pressure distribution plots. The wall pressure distribution for the centered plug followed this same trend.

## III. Discussion of Results and Comparisons

### The Axial Thrust Coefficient, $C_{f_p}$

In order to preclude modifications to the blow-down wind tunnel it was decided to test one side of each of the three possible configurations at a time. In this way the performance of the ideal nozzle was calculated by doubling the results obtained from the ideal model; the performance of the fully translated nozzle was calculated by combining the performance of the ideal model and that of the full step model; and the performance of the centered plug was calculated by doubling the performance of the one-half step model (see Fig. 2).

$C_{f_p}$ was found to remain nearly constant for all pressure ratios for both the translated and centered plugs (see Fig. 17). However, $C_{f_p}$ for the centered plug is consistently lower than the $C_{f_p}$ for the translated plug. This difference in $C_{f_p}$ is due partly to the higher values of throat pressure that were obtained for the ideal configuration, as compared to the configurations that contained a setback. The effect of a higher throat pressure would be to increase the thrust and $C_{f_p}$. $C_{f_p}$ for the translated plug was computed by adding together the axial thrusts obtained from the ideal and the fully translated configurations. The $C_{f_p}$ for the centered plug was computed by doubling its axial thrust. Thus lower values of $C_{f_p}$ were obtained for the centered plug than for the translated plug. Another reason for this is that the throat separation jet reattaches to the plug wall at a point where the local plug wall angle with respect to the direction of the jet is smaller for the centered plug than for the translated plug. Thus less compression is required to turn the flow, and the wall

pressure of the centered plug will be less than the wall pressure of the translated plug. This will occur near the throat where the greatest contribution to axial thrust is obtained.

No direct comparison can be made to the results that Barnes (Ref 3) obtained as he used only the axial thrust contribution of the plug wall in his computation. However he did find that at low pressure ratios (below 4.5) the axial thrust loss was greater for the centered plug than for the translated plug. Above a pressure ratio of 4.5 and up to approximately 6.2 Barnes found the axial thrust loss to be nearly equal for both configurations.

## Analysis of Thrust Vectoring Mechanism

To completely determine the effect of pressure ratio on $\alpha$ it would be necessary to have several more data points than were available. However some generalizations may be made. For pressure ratios equal to or greater than design, $\alpha$ appears to remain nearly constant at approximately $-0.8^{\circ}$ or to vary only slightly with pressure ratio. This trend could probably be expected to continue as only the low pressure in the setback and the oblique shock created by attachment of the separated jet are affecting the wall pressure of the translated plug for these pressure ratios. The low pressure created in the separation region was found to remain nearly constant for all pressure ratios.

The pressure rise that the oblique shock creates is seen to be nearly constant for all pressure ratios, as may be seen by examining the first data point downstream of the throat (see Figs. 10 through 15). Examination of Figs. 10 and 11 would make it appear as though $\alpha$ should be positive; however, the greater pressure shown existing on the plug

wall is offset by the higher pressure obtained at the throat for the ideal plug nozzle. As the pressure ratio decreases below the design value, $\alpha$ is influenced by a second oblique shock. This oblique shock as mentioned previously is caused by reflection of expansion waves off the upper jet boundary. As the oblique shock moves upstream with decreasing pressure ratio the pressure rise created behind the oblique shock causes $\alpha$ to rise to $+3.5^\circ$ at a pressure ratio of 18. The effect of this pressure rise on $\alpha$ is then nullified by the flow expanding downstream of the oblique shock and the appearance of a pressure rise on the wall of the ideal configuration which is caused by compressive turning. The combination of these two phenomena cause $\alpha$ to decrease rapidly to $-1.4^\circ$ at a pressure ratio of 10.

Barnes (Ref 3) found that for pressure ratios below his design pressure ratio of 7.8 that a normal shock influenced $\alpha$, in much the same manner as the oblique shock did in this investigation. The general trend of the plot of $\alpha$ as a function of pressure ratio was the same. Barnes found that as he approached the design pressure ratio (which the limit of the high pressure air supply did not allow him to reach) there was an indication that the amount of thrust vectoring would continue to increase with increasing pressure ratio. The results of this investigation do not verify that trend.

## IV. Conclusions and Recommendations

As a result of this experimental investigation the following conclusions concerning the test parameters were reached.

1) The thrust vector angle $\alpha$ is not a strong function of pressure ratio for pressure ratios above design and remains at approximately $-0.8^\circ$ in this regime.
2) Below the design pressure ratio $\alpha$ is a strong function of pressure, and varys from $-0.6^\circ$ to a high of $+3.5^\circ$ to $-1.4^\circ$ with decreasing pressure ratios.
3) The axial thrust coefficient is not a strong function of pressure ratio in the pressure ratio range covered in this experiment.
4) The step produced a sizable reduction in the axial thrust. The centered plug produced a greater reduction of axial thrust than the translated plug.

For operation at pressure ratios below the design value the thrust vector angle was too dependent upon the pressure ratio to allow for easy control of the thrust vector. For operation at pressure ratios above the design value the thrust vector is nearly constant but of too small a magnitude to allow significant thrust vectoring.

Based on the results of this experimental investigation, neither significant nor directionally consistent thrust vectoring could be obtained over the fairly broad range of pressure ratios tested. It is therefore recommended that no further research be devoted to a translating plug nozzle.

## Bibliography


1. Ciepluch, C.C., G.H. Krull, and F.W. Steffen. Preliminary Investigation of Performance of Variable-Throat Extended-Plug-Type Nozzles Over Wide Range of Nozzle Pressure Ratios. RM E53J28. Washington, D.C., NACA, 1954.

2. Berman, K., and F.W. Crimp, Jr. Performance of Plug-Type Rocket Exhaust Nozzles. Presented at the American Rocket Society Solid Propellant Rocket Research Conference, Princeton, N. J. January 28-29, 1960. ARS Preprint No. 1047-60.

3. Barnes, W.J. Thrust Vectoring with a Plug Nozzle by Plug Translation. Thesis, Air Force Institute of Technology: Wright-Patterson AFB, Ohio, August 1964.

4. Nichols, M.E. Design and Construction of a Supersonic Blow-Down Wind Tunnel. Thesis, Air Force Institute of Technology: Wright-Patterson AFB, Ohio, May 1964.

5. A.S.M.E. Special Research Committee on Fluid Meters. Fluid Meters Their Theory and Application, Part I. New York: America Society of Mechanical Engineers, 1937.

6. Conners, J.F., and R.C. Meyer. Design Criteria for Axisymmetric and Two-Dimensional Supersonic Inlets and Exits. Tn 3589. Washington, D.C., NACA, 1956.

7. Beale, W.T., and J.H. Povolny. Internal Performance of Two-Dimensional Wedge Exhaust Nozzles. RM E56D29b. Washington, D.C., NACA, 1957.

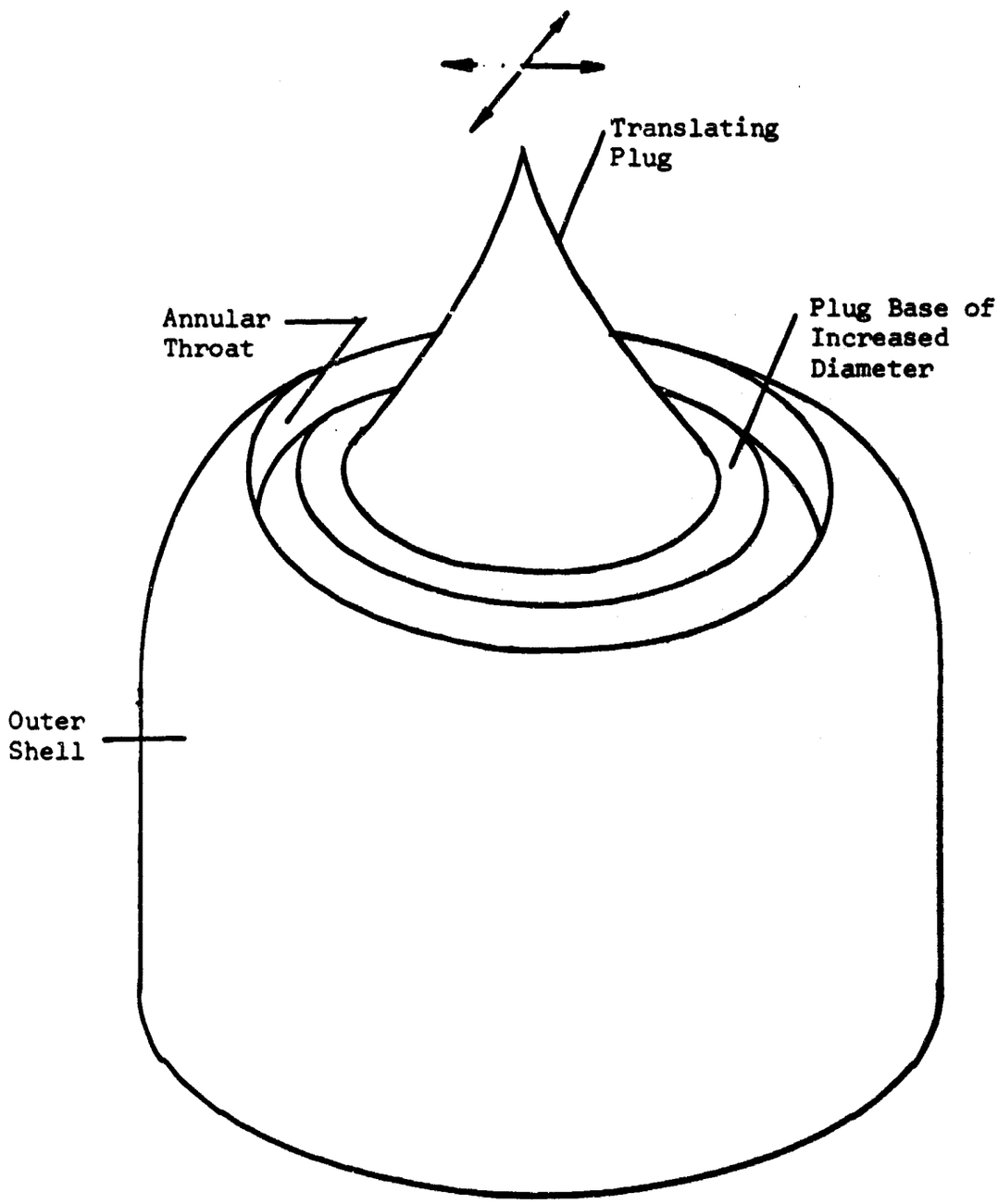


**Figure 1**

**Sketch of Three-Dimensional Plug Nozzle with Translating Plug**

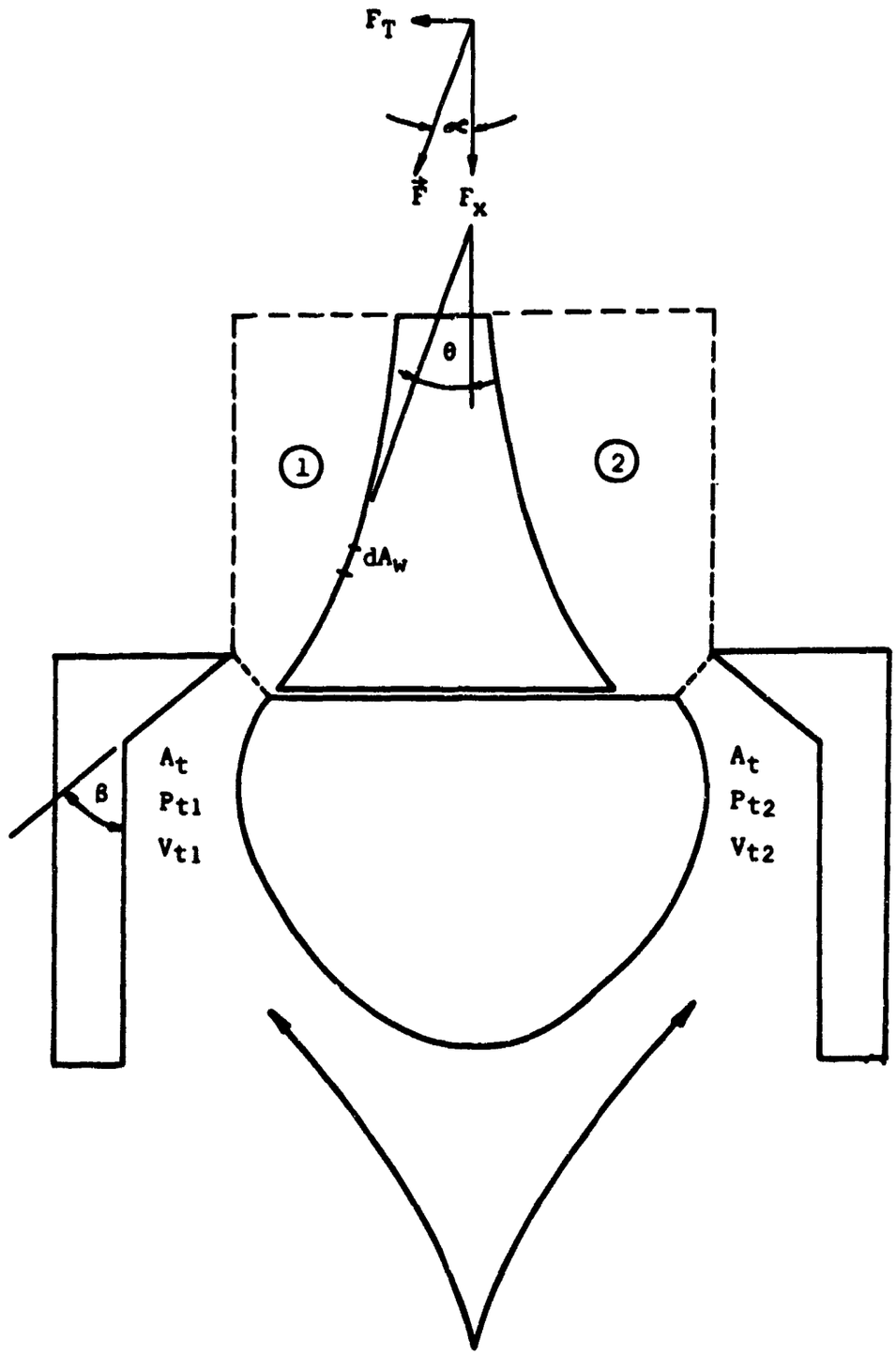


Figure 2

Two-Dimensional Plug Nozzle with Translating Plug

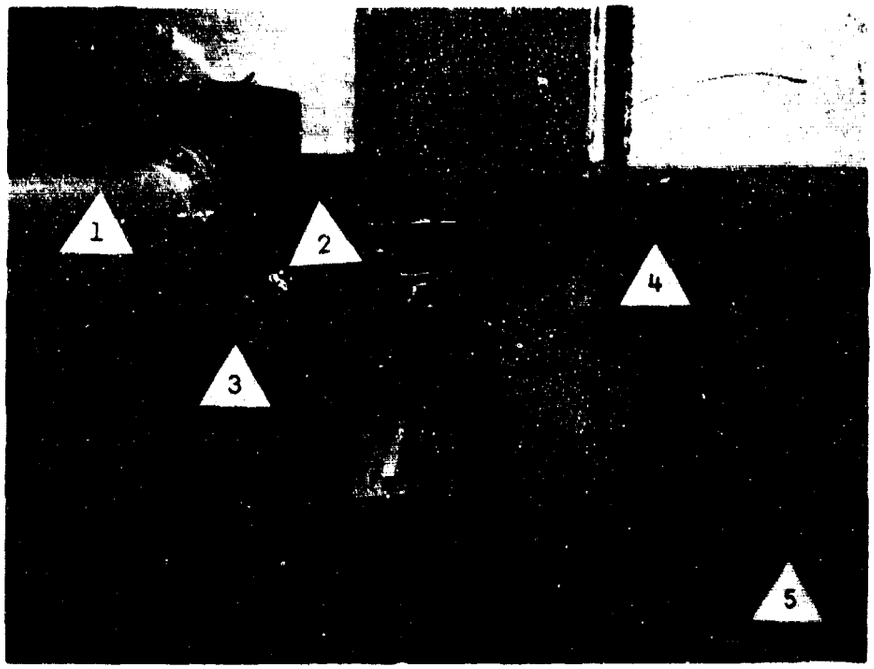


1. Settling Chamber
2. Test Section
3. Pressure Transducers
4. Schlieren Apparatus
5. Vacuum Pump

Note Visicorder not shown

Figure 3

General Arrangement of Apparatus

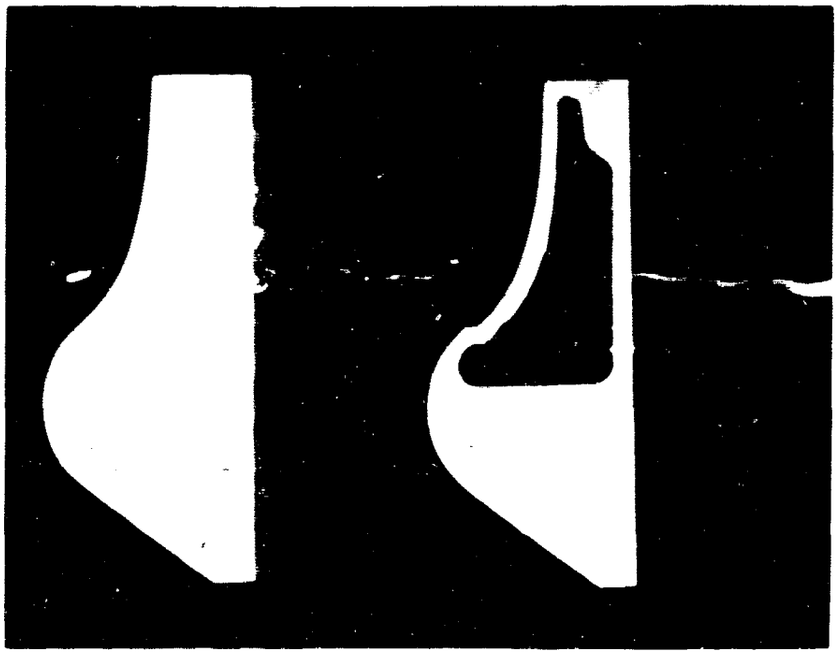

Fig. 5b
Ideal and Centered Plug Nozzles

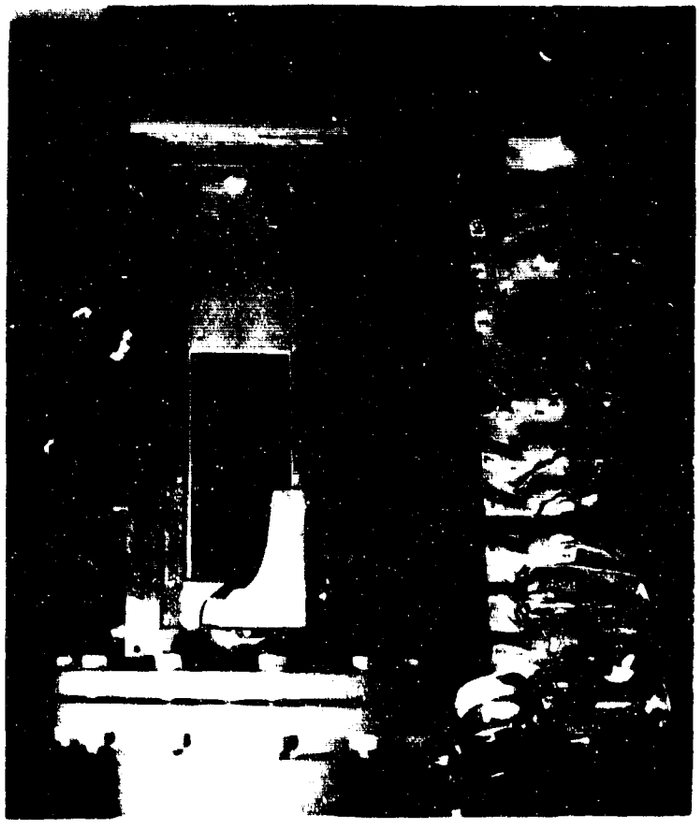

Fig. 5a
Test Section and Translated Plug Nozzle

Figure 5
Test Section and Plug Nozzles

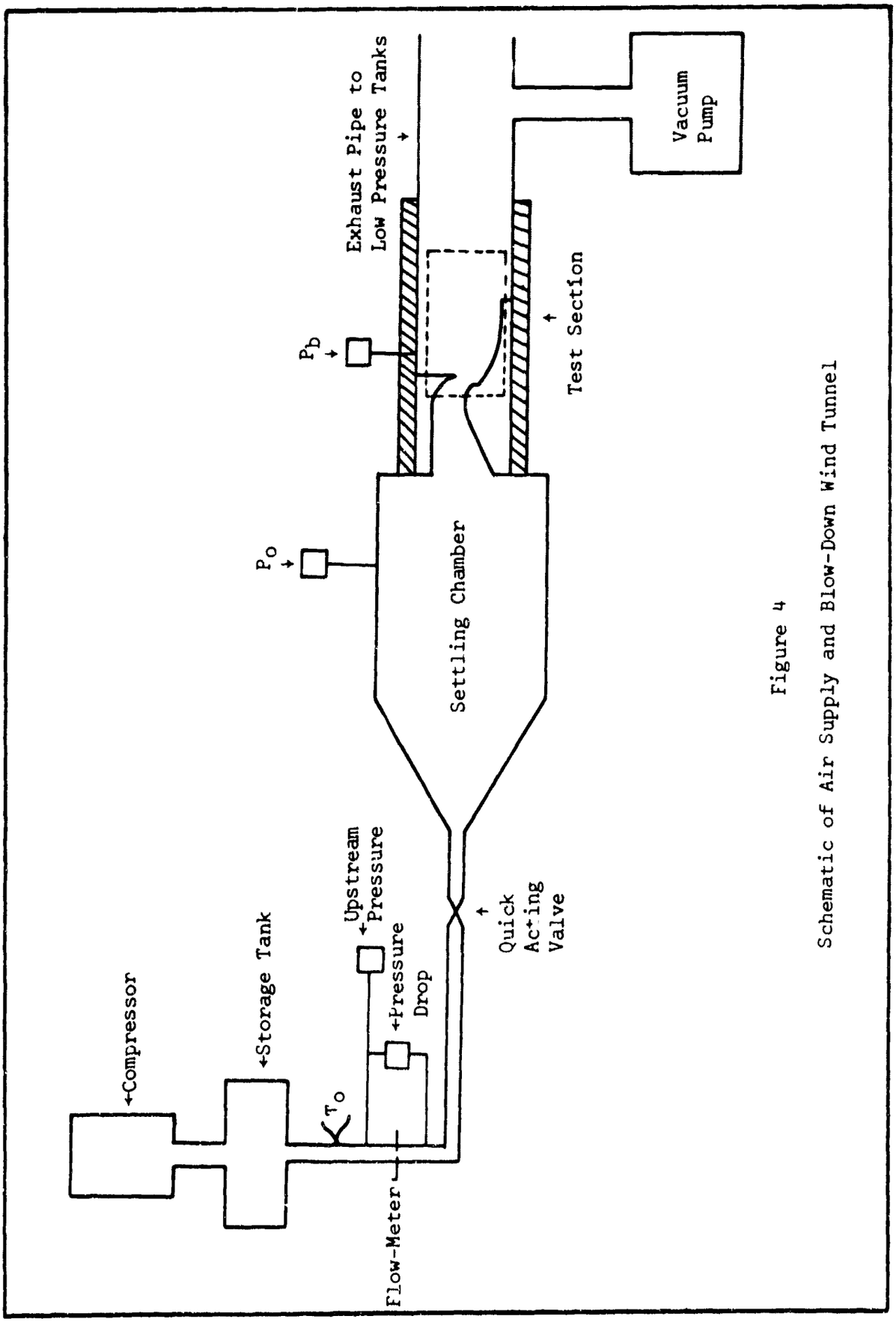


Figure 4

Schematic of Air Supply and Blow-Down Wind Tunnel

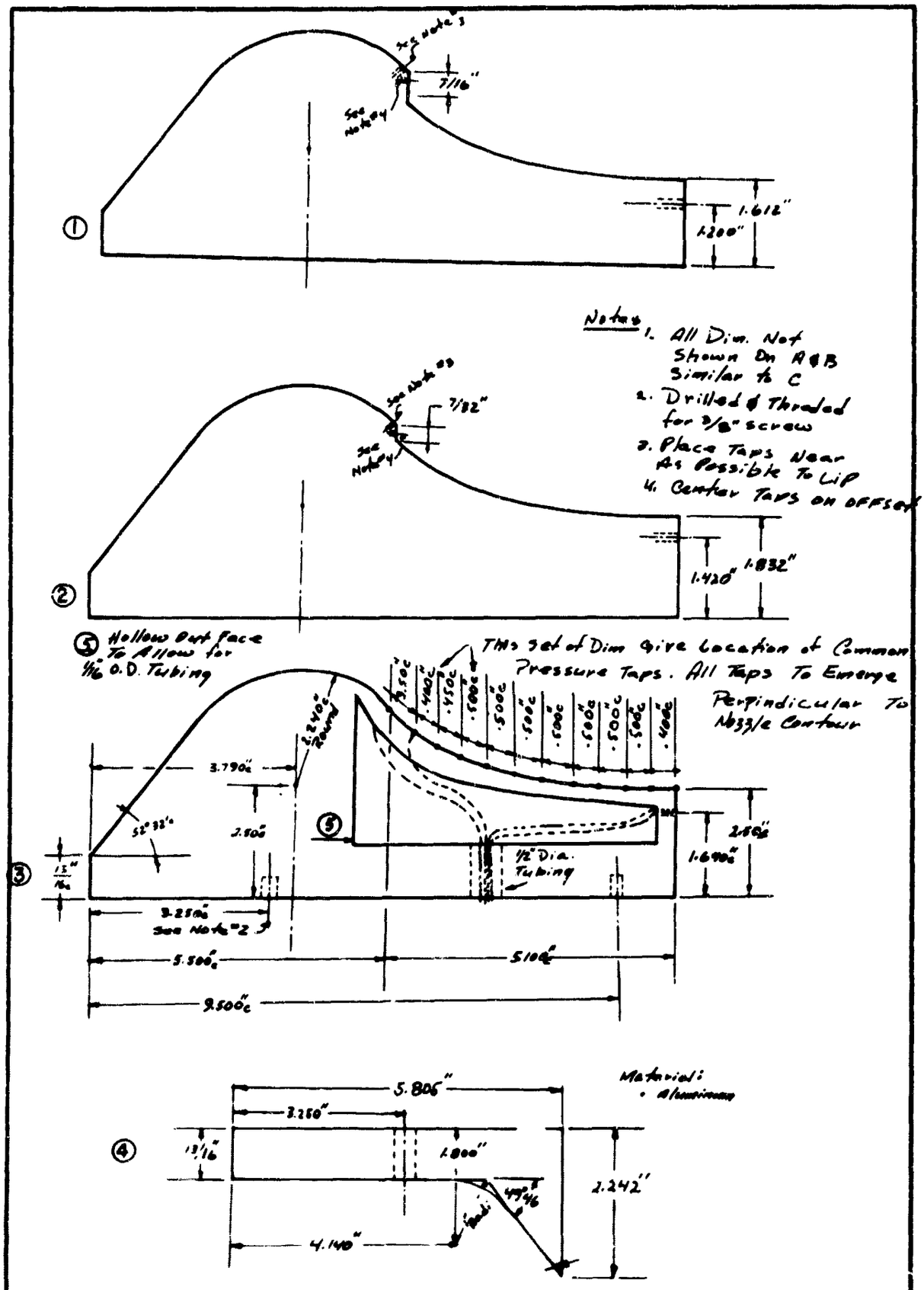


Figure 6 Dimensions of Plug Nozzles

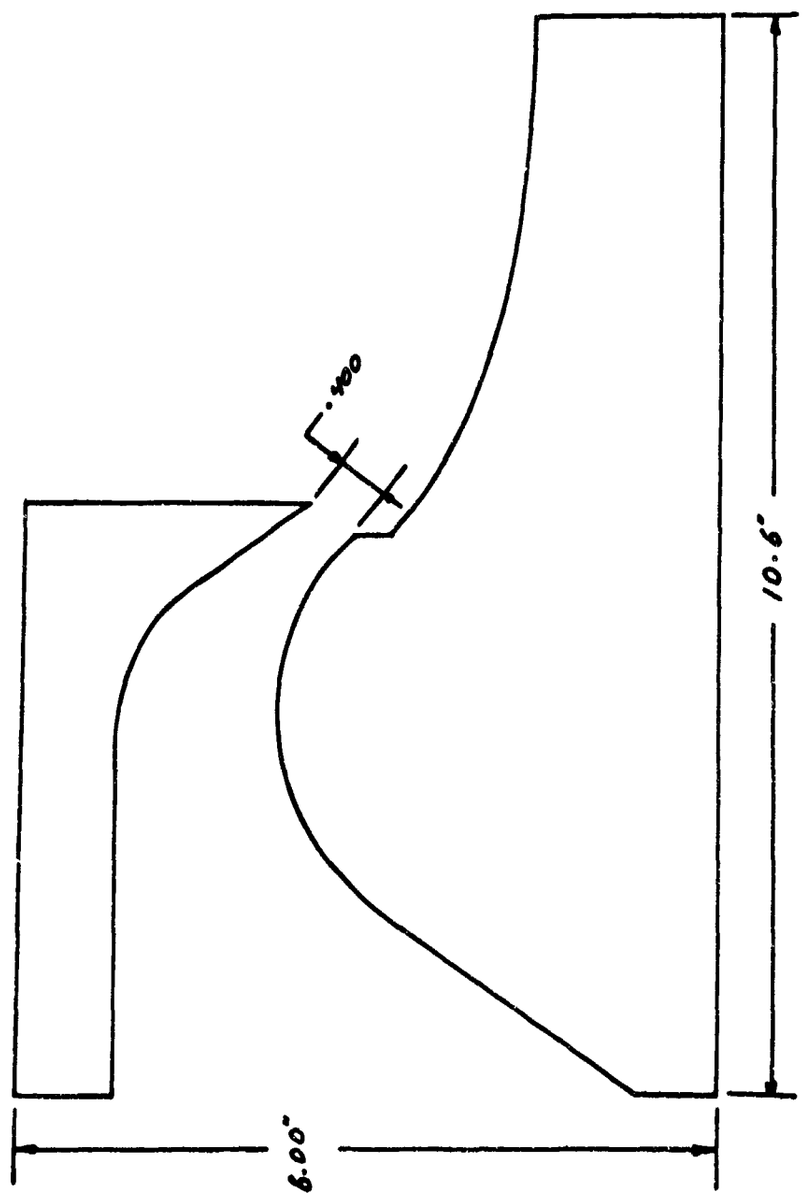


Figure 7

Plug Nozzle Assembly

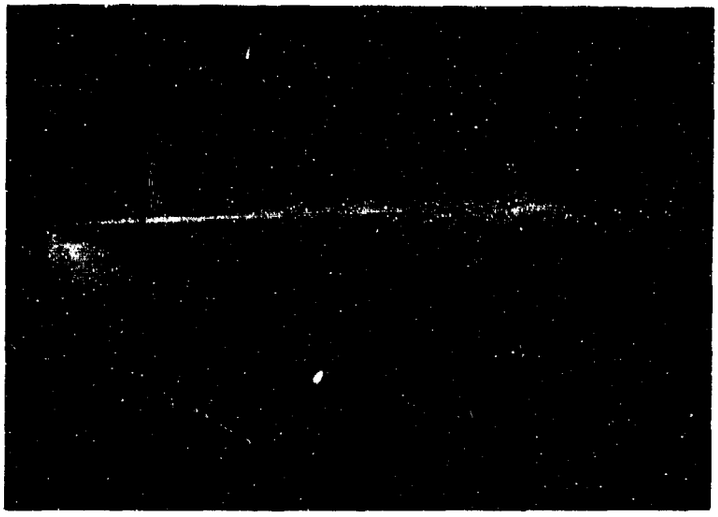

Fig. 8a
$P_o/P_b \approx 60$

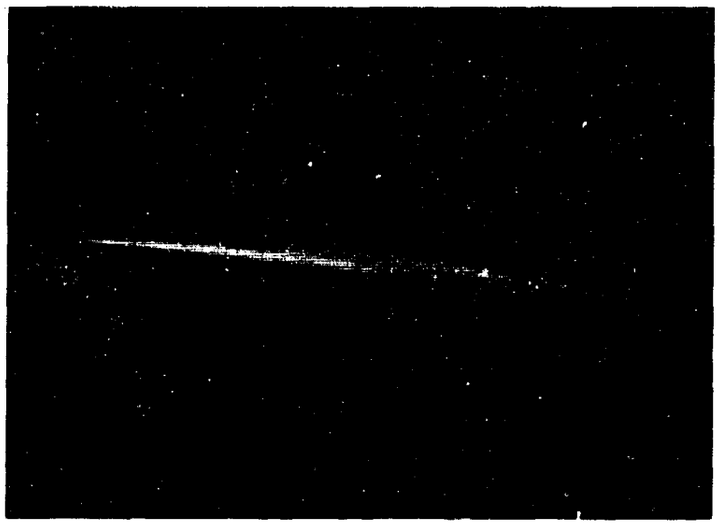

Fig. 8b
$P_o/P_b \approx 37$

Fig. 8c
$P_o/P_b \approx 18$

Figure 8
Schlieren Photographs of Ideal Plug Nozzle

Fig. 9a
$P_o/P_b \approx 60$

Fig. 9b
$P_o/P_b \approx 37$

Fig. 9c
$P_o/P_b \approx 18$

Figure 9

Schlieren Photographs of Translated Plug Nozzle

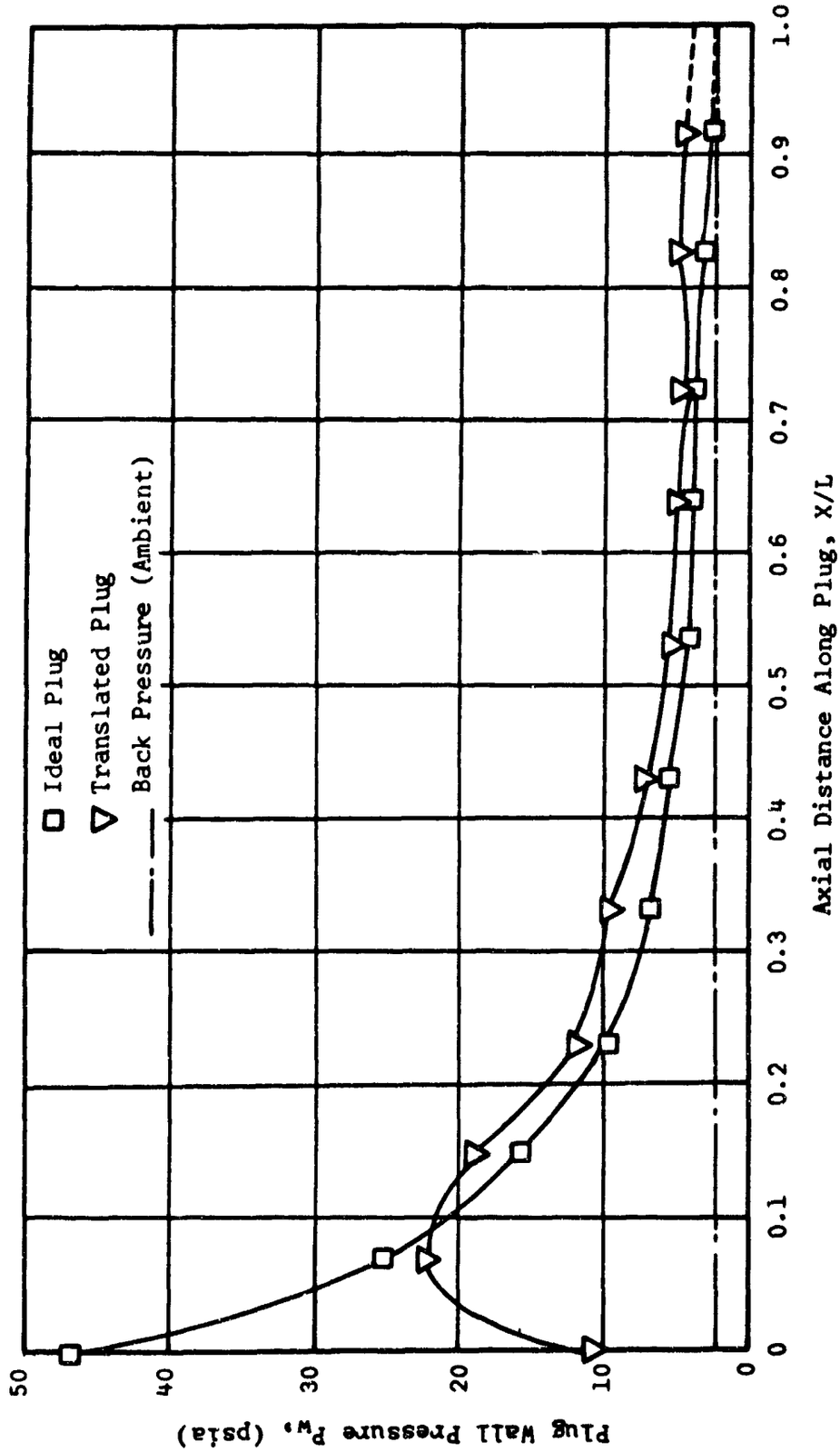


Figure 11

Experimental Plug Wall Pressure Distribution for Ideal and Translated Plug, $P_o/P_b$ = 37

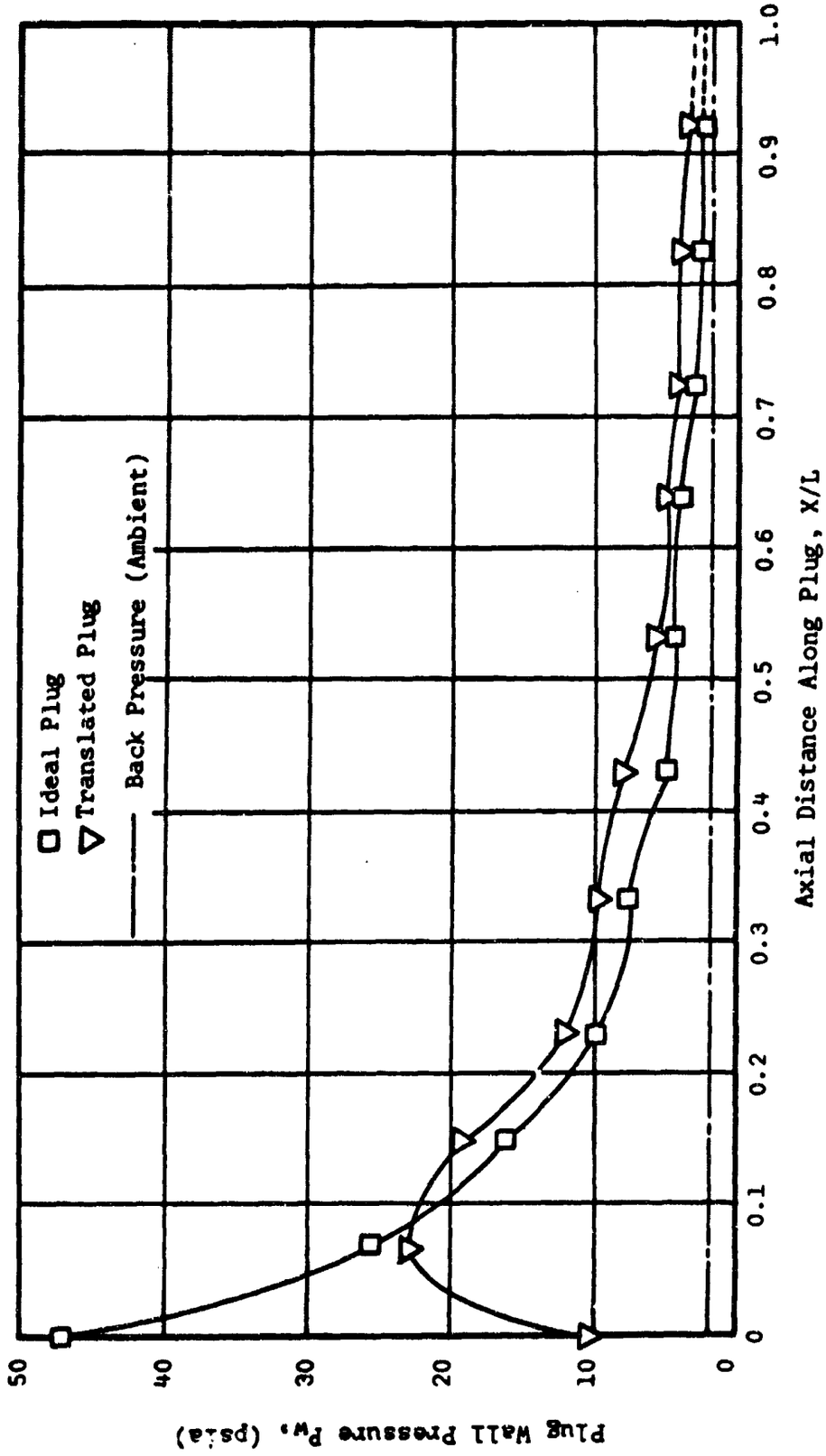


Figure 10

Experimental Plug Wall Pressure Distribution for Ideal and Translated Plug, $P_o/P_b$ = 60

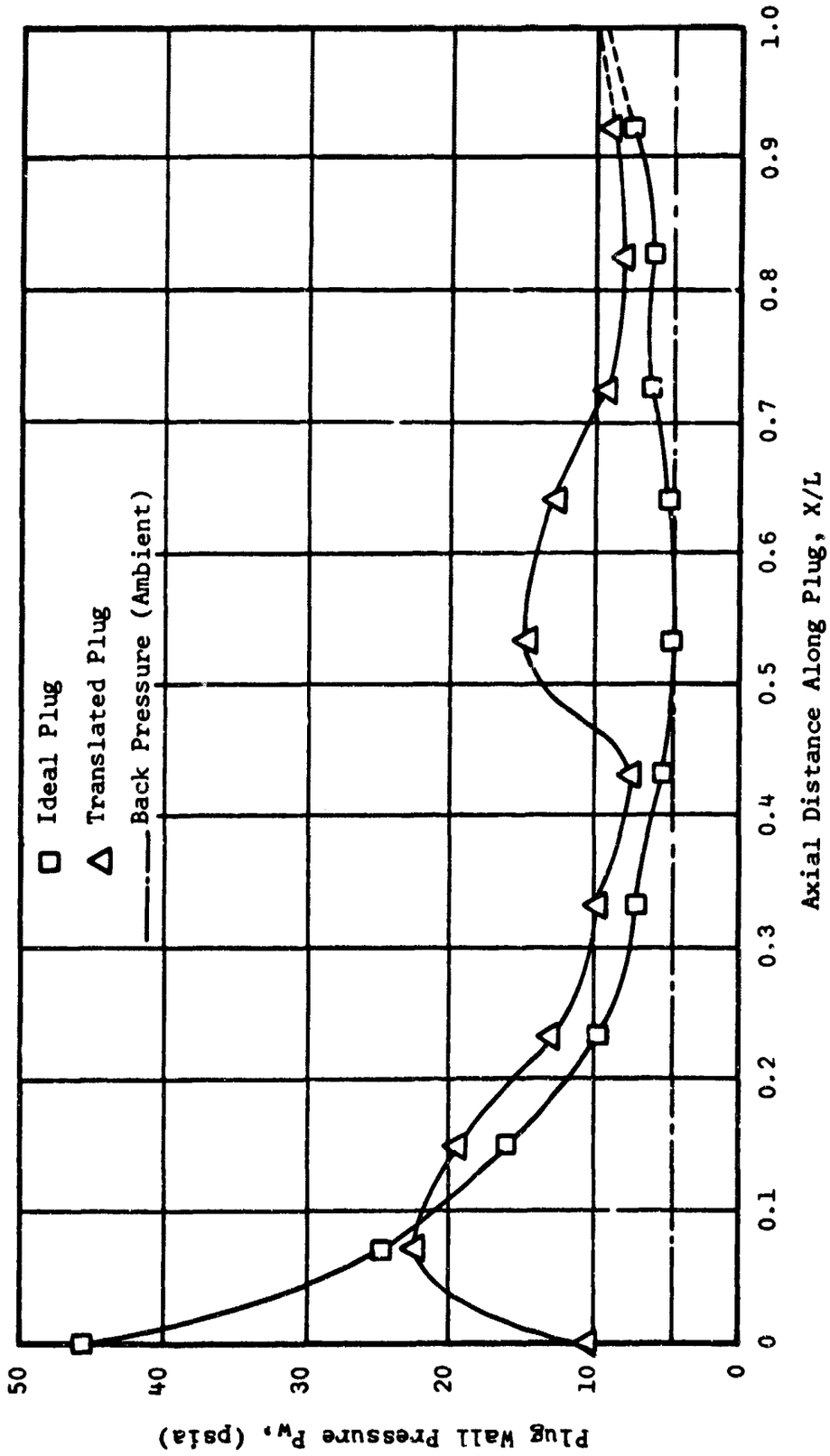


Figure 13

Experimental Plug Wall Pressure Distribution for Ideal and Translated Plug $P_o/P_b = 18$

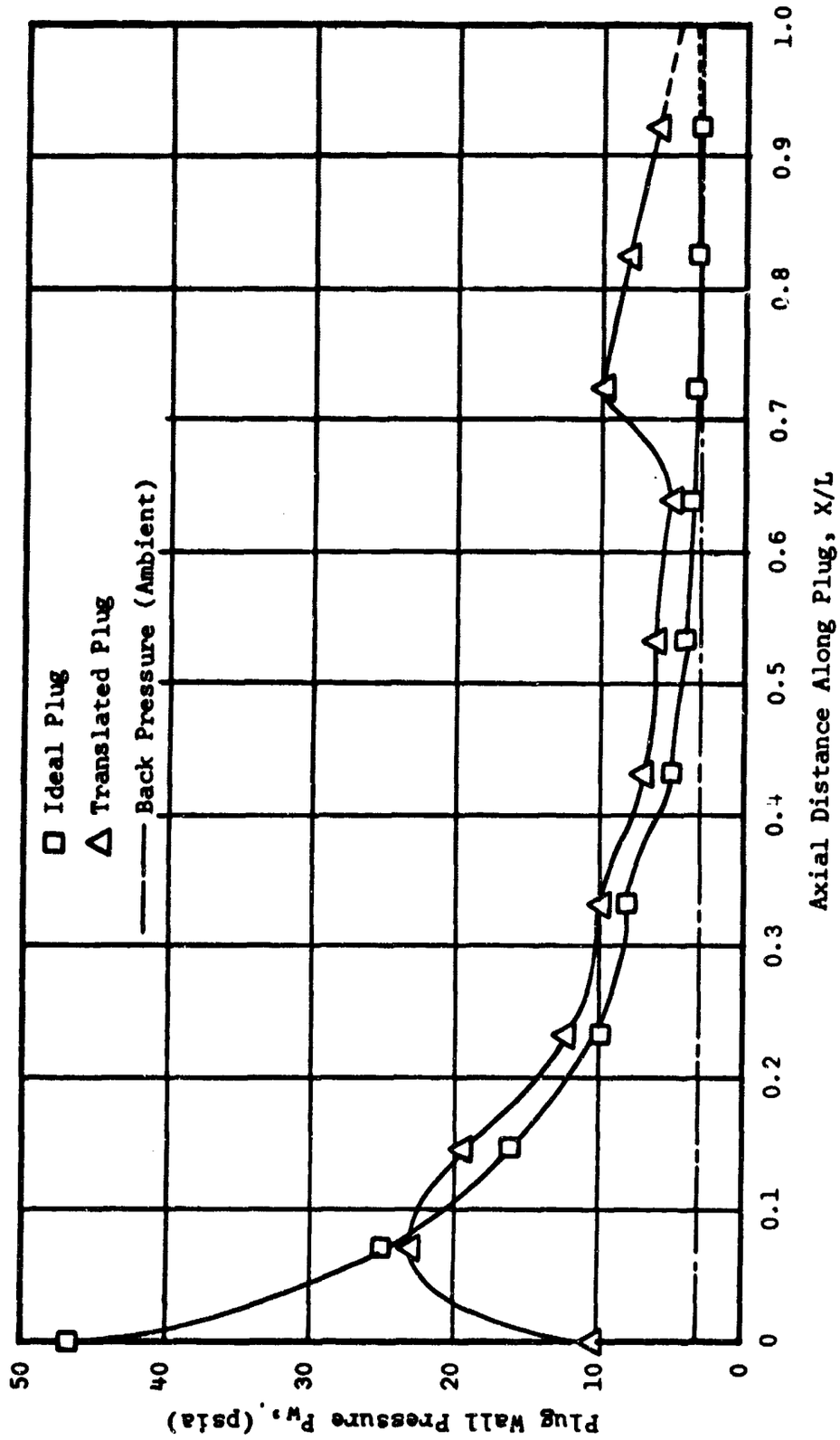


Figure 12

Experimental Plug Wall Pressure Distribution for Ideal and Translated Plug, $P_o/P_b = 30$

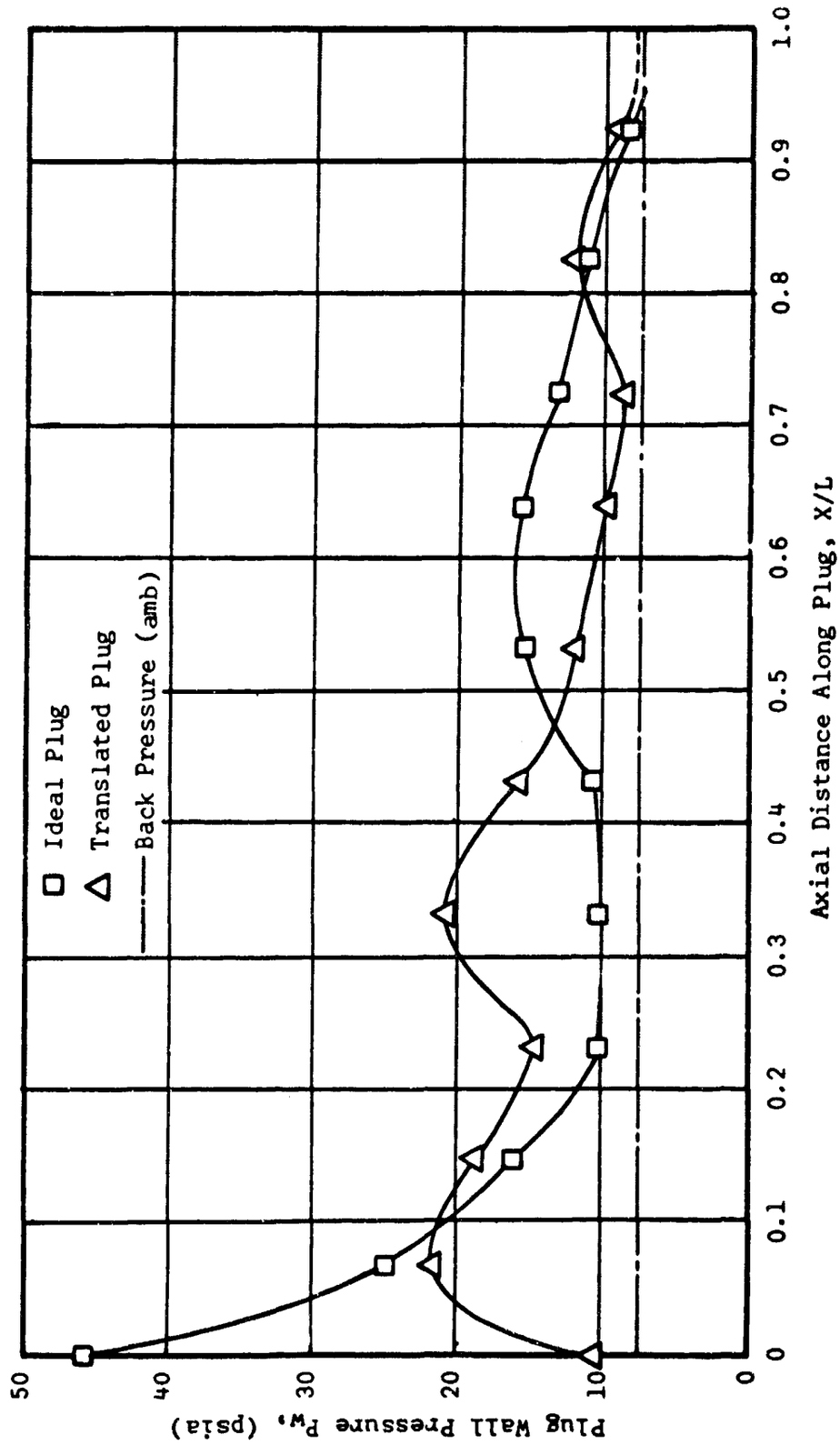


Figure 15

Experimental Plug Wall Pressure Distribution for Ideal and Translated Plug, $P_o/P_b = 10$

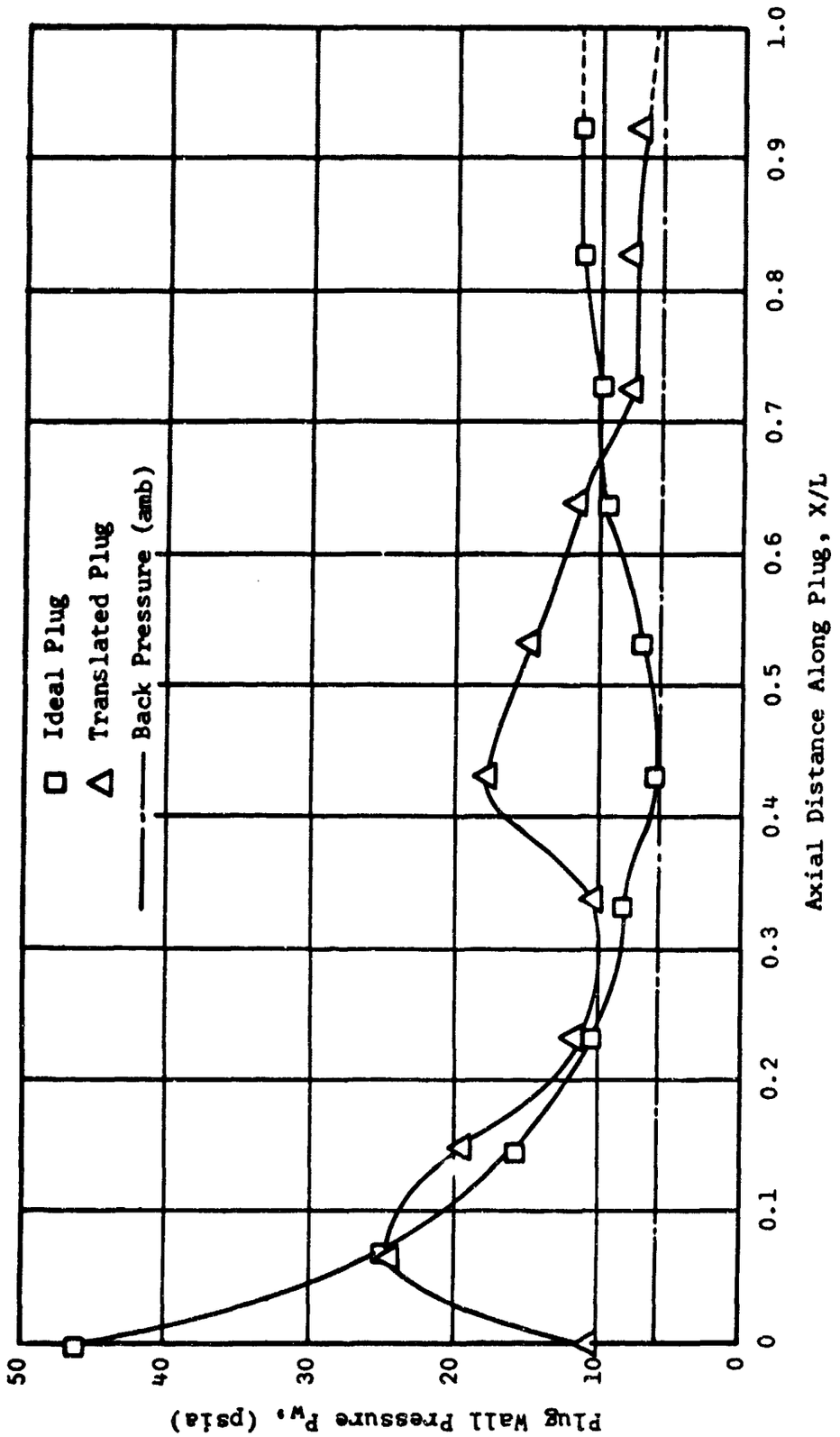


Figure 14

Experimental Plug Wall Pressure Distribution for Ideal and Translated Plug, $P_o/P_b$ = 14

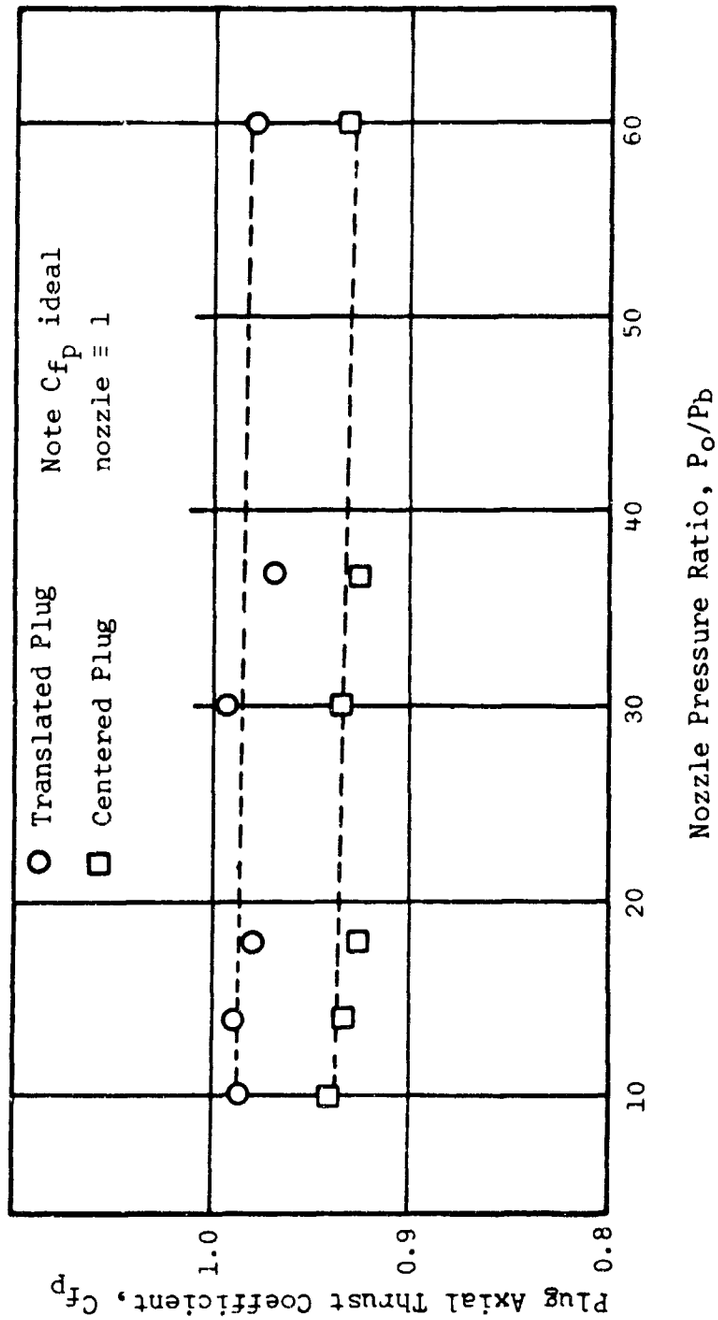


Figure 17

Variation of Axial Thrust Coefficient, $Cf_p$, with Pressure Ratio

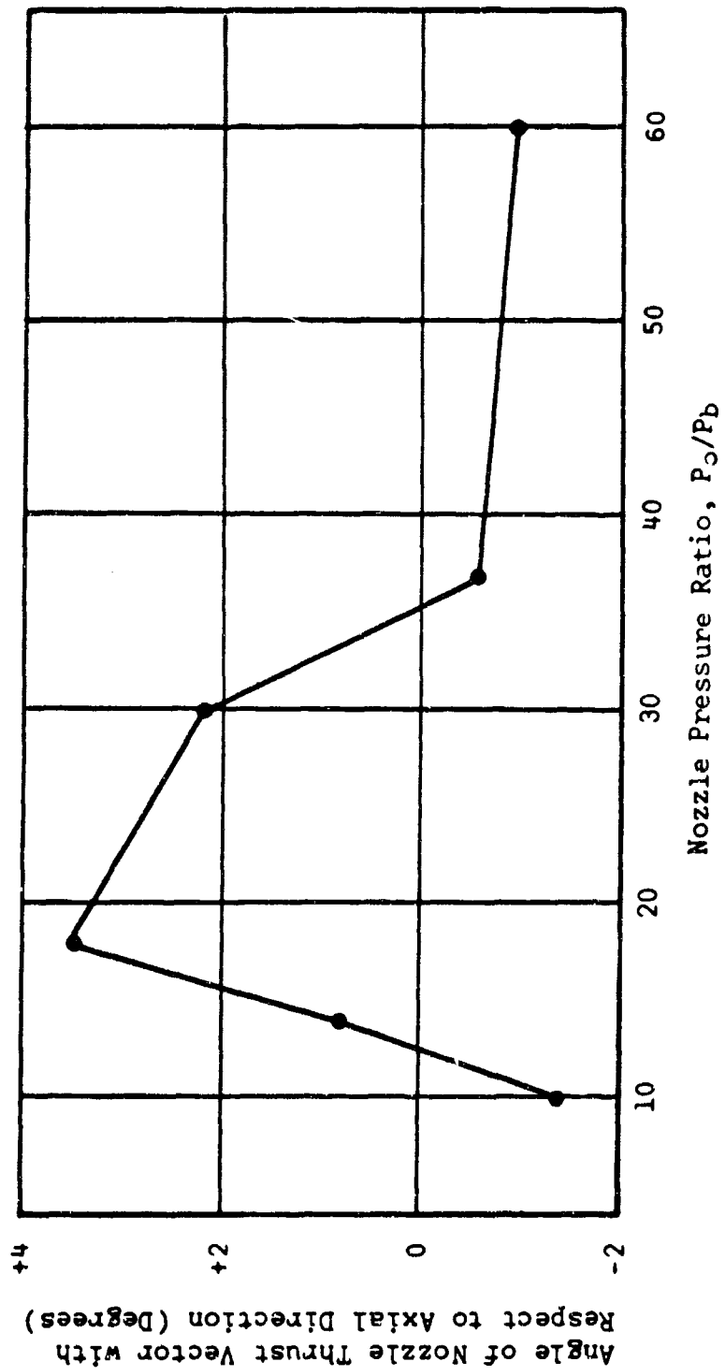


Figure 16

Variation of Thrust Vectoring with Pressure Ratio

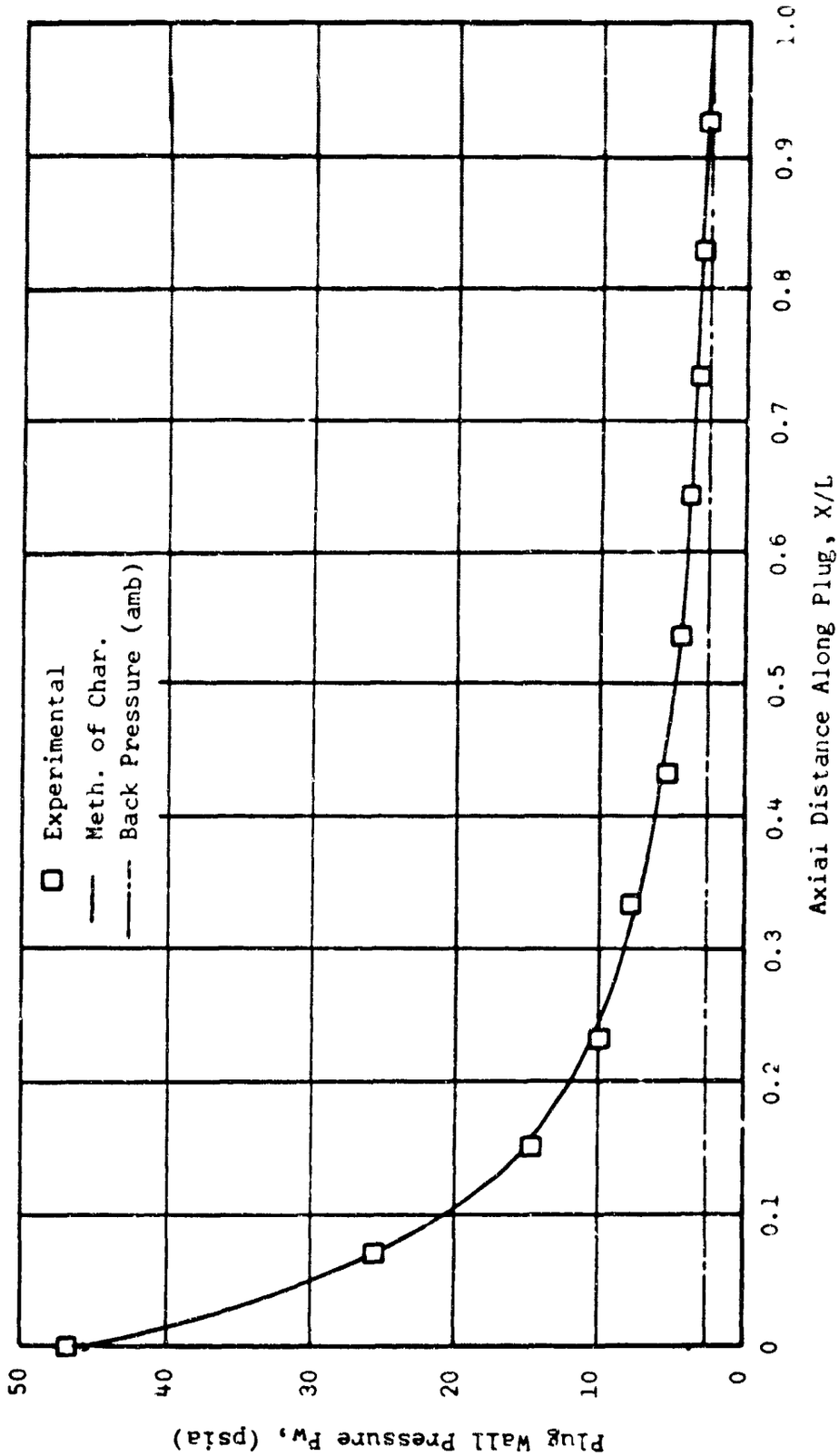


Figure 18

Comparison Between Experimental Data and Method of Characteristics, $P_o/P_b = 37$

TABLE I

Pertinent Information on Transducers, Visicorder and Amplifiers

| Transducers | | | |
|---|---|---|---|
| Manufacturer | Model # | Serial # | Range |
| Bourns | 70620-01-103 | 2376 | 0-100 psid |
| Bourns | 70620-01-103 | 2363 | 0-100 psid |
| Giannini | N-A-10-75 | 15685 | 0-100 psia |
| Giannini | N-A-10-75 | 15686 | 0-100 psia |
| Giannini | N-A-10-75 | 15690 | 0-100 psia |
| Giannini | N-A-5-75 | 12879 | 0-50 psia |
| Giannini | N-A-5-75 | 12882 | 0-50 psia |
| Giannini | N-A-3.5-75 | 15683 | 0-35 psia |
| Giannini | N-A-3.5-75 | 15682 | 0-35 psia |
| Giannini | N-A-3.5-75 | 15680 | 0-35 psia |
| Giannini | S-A-3-75 | 12877 | 0-30 psia |
| Colvin Lab. | 311-A-5-50 | 201 | 0-50 psia |
| | Visicorder | | |
| Honeywell | 906A | 96912 | ±1 in |
| | Amplifiers | | |
| Honeywell | T6GA-500A2 | 62789 | - - |
| Honeywell | T6GA-600B | H10 251 | - - |